


Heat transfer and fluid flow analysis in a realistic 16-generation lung


Cite as: Phys. Fluids **34**, 061906 (2022); <https://doi.org/10.1063/5.0093912>

Submitted: 31 March 2022 • Accepted: 21 May 2022 • Accepted Manuscript Online: 23 May 2022 • Published Online: 17 June 2022

 Suvash C. Saha,  Isabella Francis, Xinlei Huang (黄新磊), et al.

COLLECTIONS

 This paper was selected as Featured

 This paper was selected as Scilight



View Online



Export Citation



CrossMark

ARTICLES YOU MAY BE INTERESTED IN

[Experiments on turbulence from colliding ice floes](#)

Physics of Fluids **34**, 065133 (2022); <https://doi.org/10.1063/5.0088953>

[Computational fluid dynamics used to model heat transfer within lungs](#)

Scilight **2022**, 241109 (2022); <https://doi.org/10.1063/10.0011772>

[Large-eddy simulation of particle-laden isotropic turbulence using machine-learned subgrid-scale model](#)

Physics of Fluids **34**, 065129 (2022); <https://doi.org/10.1063/5.0098399>

APL Machine Learning

Open, quality research for the networking communities

MEET OUR NEW EDITOR-IN-CHIEF

LEARN MORE



Heat transfer and fluid flow analysis in a realistic 16-generation lung



Cite as: Phys. Fluids **34**, 061906 (2022); doi: [10.1063/5.0093912](https://doi.org/10.1063/5.0093912)

Submitted: 31 March 2022 · Accepted: 21 May 2022 ·

Published Online: 17 June 2022



View Online



Export Citation



CrossMark

Suvash C. Saha,^{1,a)} Isabella Francis,¹ Xinlei Huang (黄新磊),¹ and Akshoy Ranjan Paul²

AFFILIATIONS

¹School of Mechanical and Mechatronic Engineering, Faculty of Engineering and Information Technology, University of Technology Sydney, Sydney, NSW, Australia

²Department of Applied Mechanics, Motilal Nehru National Institute of Technology Allahabad, Prayagraj, Allahabad 211004, Uttar Pradesh, India

^{a)}Author to whom correspondence should be addressed: Suvash.Saha@uts.edu.au

ABSTRACT

Heat transfer between inhaled hot/cool air and the lung surface within the human respiratory system is an intriguing topic that has not received enough attention. The lung can be considered an *in vivo* heat exchanger, balancing the inhaled air temperature by lowering the hot air temperature and increasing the cool air temperature. The current work studies the unsteady and incompressible airflow motion and heat transfer during inhalation between the surface of the lungs (37 °C) and the inhaled cool air (25 °C) in one case and inhaled hot air (43 °C) in another. Computerized tomography scan (CT-scan) images of the lung of a 39-year-old male patient were processed to generate the airway geometry consisting of 16 generations. The geometry was further modified in UG NX 12.0, and the mesh generation was carried out using Ansys Meshing. The shear stress transport (SST) $k - \omega$ turbulent model was employed in Ansys Fluent 20.2 to model the air/lung convective volume heat transfer utilizing a realistic breathing velocity profile. Temperature streamlines, lung volume temperatures, surface heat flux, and surface temperatures on all 16 generations were produced for both cases during the breathing cycle of 4.75 s. Several conclusions were made by studying and comparing the two cases. First, heat transfer between inhaled hot or cool air and the lung surface mainly occurred in the first few generations. Second, airflow temperature patterns are dependent on the inlet breathing velocity profile. Third, the lung volume temperature change directly correlates with the temperature difference between air and the lung surface. Finally, the surface heat flux strongly depended on the heat transfer coefficient. The density, viscosity, thermal conductivity, and specific heat of hot/cool air affected the Reynolds number, Nusselt number, heat transfer coefficient, and surface heat flux.

Published under an exclusive license by AIP Publishing. <https://doi.org/10.1063/5.0093912>

I. INTRODUCTION

Many unnatural heat transfer phenomena in medical applications, such as radio-frequency ablation (Iasiello *et al.*, 2020), microwave ablation and electromagnetic field (Keangin and Rattanadecho, 2013; Keangin *et al.*, 2013), and laser angioplasty (Iasiello *et al.*, 2019), are crucial for the reduction and treatment of cancerous cells and blood and heart diseases. Interestingly, a natural heat transfer phenomenon occurs inside the lungs that prevents alveolar lung injury. However, this process cannot be demonstrated through computerized tomography (CT)-scanned images, and thus computational methods are required. The massive development of computational techniques in the last few decades enabled researchers to study complex biomedical phenomena. Computational fluid dynamics (CFD) is used as a robust tool to predict the flow characteristics in the various vital human organs, including the lungs (Srivastav *et al.*, 2011a; Faizal *et al.*, 2020). The major studies that

involved CFD in the lungs included particle transport (Srivastav *et al.*, 2011b; Paul *et al.*, 2021; Larpruenrudee *et al.*, 2022), drug deposition (Shukla *et al.*, 2013; Srivastav *et al.*, 2019a), lung performance at different breathing conditions (Srivastav *et al.*, 2016; Tiwari *et al.*, 2021a), compliant lung walls (Srivastav *et al.*, 2021), diseased lung airways (Singh *et al.*, 2021), and even design of inhaler devices (Tiwari *et al.*, 2021b; Tiwari *et al.*, 2022). It is, however, curious to find that although some scattered studies reported in the literature (Daviskas *et al.*, 1990; Kulkarni and Kleinstreuer, 2020), heat and mass transfer within the human respiratory system were not studied invariably to date. Due to the recent outbreak of severe acute respiratory syndrome coronavirus 2 (SARS-CoV-2), the topic is now at the center of biomedical research (Islam *et al.*, 2021a, 2021b; Pan *et al.*, 2021; Xu *et al.*, 2021).

This study attempts to gather the efforts of the numerous researchers to the progress of the topic, both mathematically and

experimentally. [Hanna and Scherer \(1986\)](#) applied a quasi-steady one-dimensional theoretical model to investigate heat vapor and water losses in the respiratory tract. They explored that the most heat and mass transfer occur in the first several generations of the lung. They published another paper with a similar theoretical model. They found that the two leading factors of the respiratory air-conditioning process are the blood temperature distribution along the airway wall and the total cross-sectional area. [Tsu et al. \(1988\)](#) developed a one-dimensional theoretical model to describe the exchange of heat, mass, and soluble gas in human airways. Their model takes into account the fact that these three exchange processes occur simultaneously and influence each other. [Daviskas et al. \(1990\)](#) developed a time-dependent single differential model to calculate the heat and water vapor transport in upper airways. The results of the computed data agreed well with the experimental data. [Finlay and Stapleton \(1995\)](#) developed equations to couple the heat and mass transfer between the discrete and continuous phases in their investigation of the relationship between the deposition of hygroscopic droplets and their surrounding phases. They concluded that the effect of coupling is insignificant. [Primiano et al. \(1988\)](#) carried out an experiment to measure the water vapor partial pressure and temperature data on healthy and cystic fibrosis (CF) patients. A total of 13 subjects participated in the investigation. In the end, they found no apparent difference in water vapor partial pressure and temperature between normal and CF patients. [Keck et al. \(2000\)](#) conducted an experiment to measure the nasal cavity temperature profile of 50 volunteers. Their experimental data provides valuable information for the validation of computational simulation.

There has been a rising trend of using numerical methods to study heat and mass transfer in human lungs. [Ingenito et al. \(1986\)](#) adopted a numerical heat transfer model to predict the experiment outcomes. Their simulations discovered the relation between inspired air temperature, minute ventilation, and heat loss in airways. [Ferron et al. \(1988\)](#) used the numerical method, calculating inhalation and exhalation in the nasal and oral cavity to estimate the growth and deposition of hygroscopic aerosols. However, due to the uncertainties they admitted, no conclusion was drawn. [Zhang and Kleinstreuer \(2003\)](#) studied airflow and heat transfer in human upper airways with a numerical model from the oral cavity to the third generation of the bronchial tree. In their paper, the relation between breathing modes and heat transfer effects was investigated, and local as well as averaged overall Nusselt number was calculated. [Tawhai and Hunter \(2004\)](#) used one symmetrical and one anatomical model with multiple layers to study the heat and water vapor transfer in human airways. Heat transport was simulated both axially and radially. Apart from water vapor transfer data, their simulations provided valuable information for the analysis of intubated airway conditions. A six-generation multi-detector row computed tomography (MDCT)-based realistic lung model was built by [Wu et al. \(2014\)](#) to investigate the local distribution of temperature and water vapor transfer within human airways. They calculated several fluid dynamic characteristics such as Nusselt number, Sherwood number, and Reynolds number. Apart from providing the precise temperature and humidity profile data, it is suggested that their simulation can also be used to estimate local convective heat and mass fluxes. [Xi et al. \(2016\)](#) reconstructed a nose and upper trachea model from magnetic resonance imaging (MRI) images. They studied the relationship between nostril orientation and airflow dynamics, heat exchange, and particle deposition. The results

show that nostril orientation influences local particle deposition, temperature, and wall heat flux. [Chen et al. \(2019\)](#) used an artificial triple bifurcation airway model to study the effects of temperature and humidity on the transport and deposition of hygroscopic aerosols in human lungs. In the end, they concluded that heat and mass transfer of the airway boundary could help estimate the deposition of hygroscopic aerosols. [Kulkarni and Kleinstreuer \(2020\)](#) constructed a computed tomography (CT)-based upper airway model from the mouth down to the third generation of the bronchial tree to study the effects of high-temperature airflow on the mucus layer. Their numerical simulations provided a large volume of data to illustrate the potential hazard of inhaling high-temperature air. [Xu et al. \(2021\)](#) conducted a numerical study to investigate the effects of ambient temperature and humidity on the transportation and deposition of hygroscopic particles in a human airway model. Based on CT scans, they developed a realistic human airway model from the nasal cavity to the fifth-generation bronchi. Moreover, they constructed a two-layer airway boundary called mucus-tissue configuration to calculate mucus-related parameters such as convection, conduction, and latent heat loss.

The above literature survey shows that intermittent works spanning over three decades were reported on the heat transfer effects in the lungs. However, the lung was not studied as an *in vivo* heat exchanger in all literature presented here. Hence, in the present study, the aim is to consider the lung as an *in vivo* heat exchanger, balancing the inhaled air temperature by lowering the hot air temperature and increasing the cool air temperature. The current work computationally investigates the unsteady and incompressible airflow motion and heat transfer during inhalation between the surface of the lungs (37 °C) and the inhaled cool air (25 °C) in one case and inhaled hot air (43 °C) in another.

II. GEOMETRY

A CT scan operation on a 50-year-old male patient's chest enabled the extraction of 513 thin-layer images in the format of Digital Imaging and Communications in Medicine (DICOM). Information regarding the CT images is listed in [Table I](#). These DICOM-formatted images are then imported to Mimics Medical 21.0 to generate the airway surface geometry in the stereolithographic (STL) format [[Fig. 1\(a\)](#)]. However, the quality of the geometry is not ideal because of high image noise and low resolution. Therefore, Geomagic Studio 2013 was used to post-process the STL file [[Fig. 1\(b\)](#)], removing abnormal features such as leaks [[Fig. 2\(a\)](#)], self-intersections [[Fig. 2\(b\)](#)], and small tunnels [[Fig. 2\(c\)](#)]. Another essential function of Geomagic Studio is reconstructing the surface in a different way. The surface pieces can be divided based on generation, thus allowing

TABLE I. Parameters of the CT scanner and CT images.

Scanner	NeuViz16 Classic
X-ray tube current	185 mA
Kilovoltage peak	120 kv
Slice thickness	1.25 mm
Spacing between slices	0.625 mm
Spatial resolution	0.35 mm
Pixels in row	512
Pixels in column	512

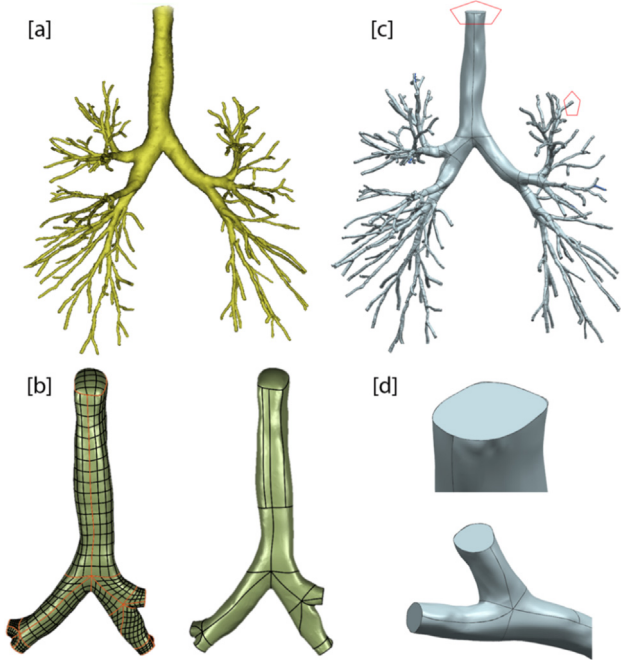


FIG. 1. (a) Full view of the geometry from Mimics Medical 21.0. (b) Surface reconstruction in Geomagic Studio 2013. (c) Post-processing in UG NX 12.0. (d) An enlarged view of the inlet and outlet created in UG NX 12.0.

generation-specific analysis. The geometry was further modified in UG NX 12.0 to make it suitable for mesh construction [Fig. 1(c)]. Using UG NX, a plane was cut at the top of the trachea and the end of each bronchiole to create an inlet and 154 outlets [Fig. 1(d)]. Figure 3 presents a 16-generation lung model according to Weibel dichotomous morphometry.

III. GRID GENERATION

Using Ansys Meshing, the accuracy of the simulation results was ensured by comparing fluid flow parameters of six mesh sizes, from a coarse mesh of 5.2×10^6 unstructured tetrahedral volume elements to

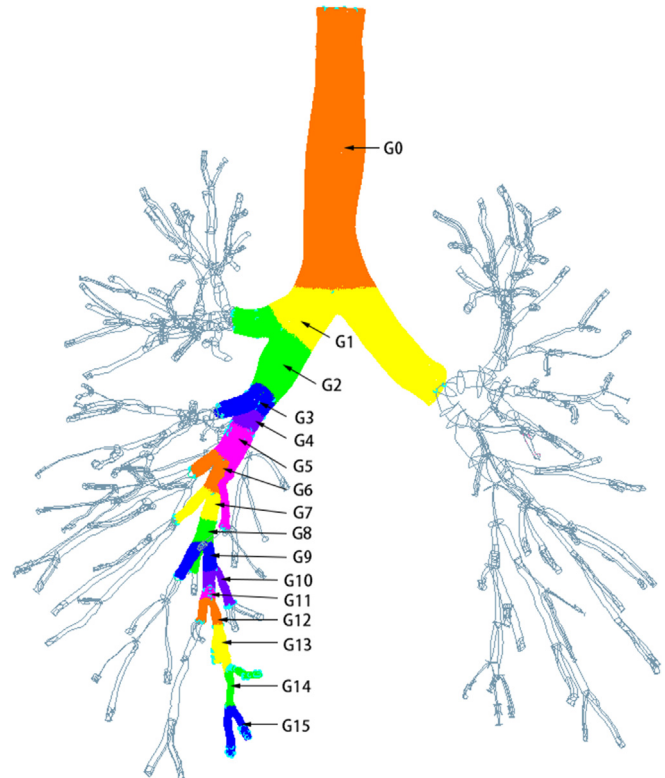


FIG. 3. A 16-generation lung model with one colored path to differentiate each generation.

a very fine mesh with 16.5×10^6 volume elements. The 16.5×10^6 volume elements of the entire tracheobronchial tree model are shown in Fig. 4(a), with an enlarged view of the carina in Fig. 4(b). The dynamic pressure and the velocity magnitude at an x - y plane cutting the trachea (gen 0) of the lung at -517.4 mm [Fig. 4(d)] and -590 mm [Fig. 4(c)], respectively, were chosen to assess and compare the six mesh sizes ($5.18, 8.17, 9.29, 11.4, 14.47,$ and 16.57×10^6) (Fig. 5). The chosen fluid flow parameters exhibit constant values at

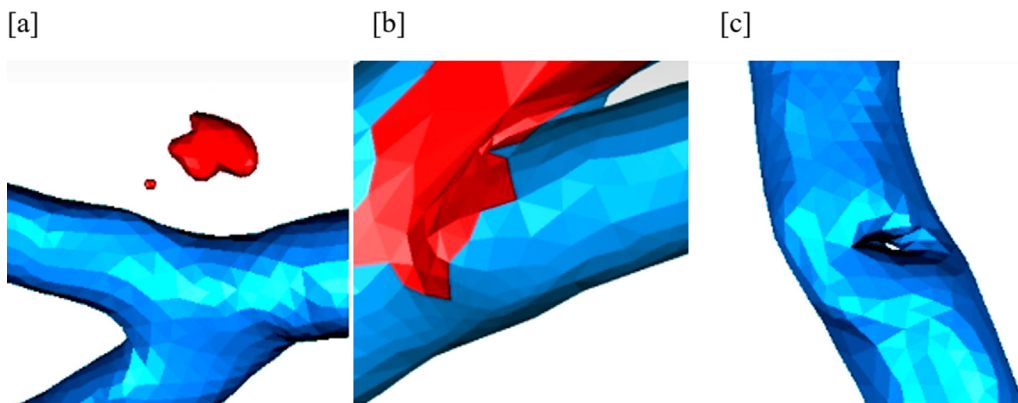


FIG. 2. (a) An example of leaks/small components error. (b) An example of self-intersection error. (c) An example of a small tunnel error.

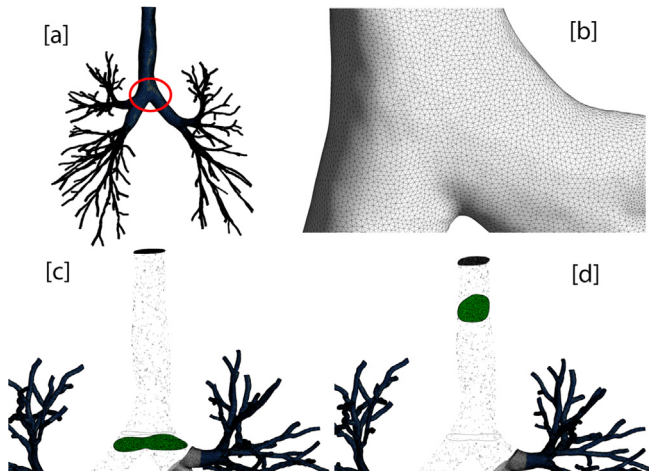


FIG. 4. (a) Fine meshing with 16.5×10^6 mesh volume elements. (b) Zoomed-in view at the tetrahedral face mesh at the trachea bifurcation (gen 0 to gen 1). (c) x - y plane at gen 0 bifurcation for the calculation of the velocity magnitude (m/s). (d) x - y plane in gen 0 for the calculation of the dynamic pressure (Pa).

around 15×10^6 mesh volume elements. Therefore, a mesh size of 16.57×10^6 mesh volume elements is selected for increased accuracy.

IV. NUMERICAL METHODS

This study uses a commercial finite volume program, Ansys Fluent 20.2 (Canonsburg, PA), to reproduce the unsteady and incompressible airflow motion and heat transfer during inhalation. The computational mesh generation was carried out using ANSYS Meshing (Ansys Inc.). A user-defined function (UDF) was developed to generate realistic high-order polynomial breathing velocity profiles for inhalation and exhalation with a total breathing cycle time of 4.75 s. The UDF is hooked at the inlet of the lung model as a velocity boundary condition, and the outlets are considered zero-pressure outlets. The surface of the lung is modeled as a 5 mm-thick wall (Chekan et al., 2016) with 1-layer shell conduction (virtual solid layer) to include heat conduction in all directions. The air backflow temperature at the outlets of the lung (exit of gen 15) is taken the same as the lung surface

temperature. Surfaces of gen 0 to gen 15 have a temperature of 37°C (310 K), the same as our body temperature. The lung surface properties are the same as *in vivo*, with a density of 250 kg/m^3 (Van Dyk et al., 1982), the specific heat of $3886 \text{ J/kg}\cdot\text{K}$, and thermal conductivity of $0.2 \text{ W/m}\cdot\text{K}$ (Yang and Cao, 2020).

Heat transfer to and from the lungs is modeled using energy conservation equations for hot and cool cases with a time step size of 0.005 s for a total time of 4.75 s. The Reynolds numbers at the inlet of the trachea for hot and cool air are 3161 and 3348, respectively. These numbers correspond to an inlet trachea diameter of 18.08 mm and an average inlet velocity of 2.892 m/s. Therefore, with a wall $y^+ < 1$, the Reynolds averaged Navier–Stokes simulation (RANS) two-equation turbulent model, SST $k - \omega$, is applied with curvature correction and energy production limiter (Srivastav et al. 2019b). A pressure–velocity coupling scheme, PISO (pressure-implicit with splitting operators), with skewness and neighbor correction of 2, and a second-order pressure spatial discretization, PRESTO, are employed (Kumar et al., 2019). Due to the slight temperature difference between the surface of the lungs (37°C) and the hot air (43°C) or cool air (25°C) flowing into gen 0 (trachea), the Boussinesq model is used to calculate the buoyancy force where density changes that are not related to buoyancy are neglected. Table II shows air properties, including density, thermal conductivity, dynamic viscosity, specific heat, and thermal expansion coefficient for the simulation of inhaled hot and cool air into the trachea (inlet) of the lung.

A. Governing equations

The continuity, momentum, and energy governing equations used to capture the unsteady, turbulent, and incompressible airflow are the following:

Continuity equation:

Using the Boussinesq model, the density variation in the continuity equation is eliminated, and hence, the equation reduces to

$$\frac{\partial u_i}{\partial x_i} = 0. \tag{1}$$

Momentum equation:

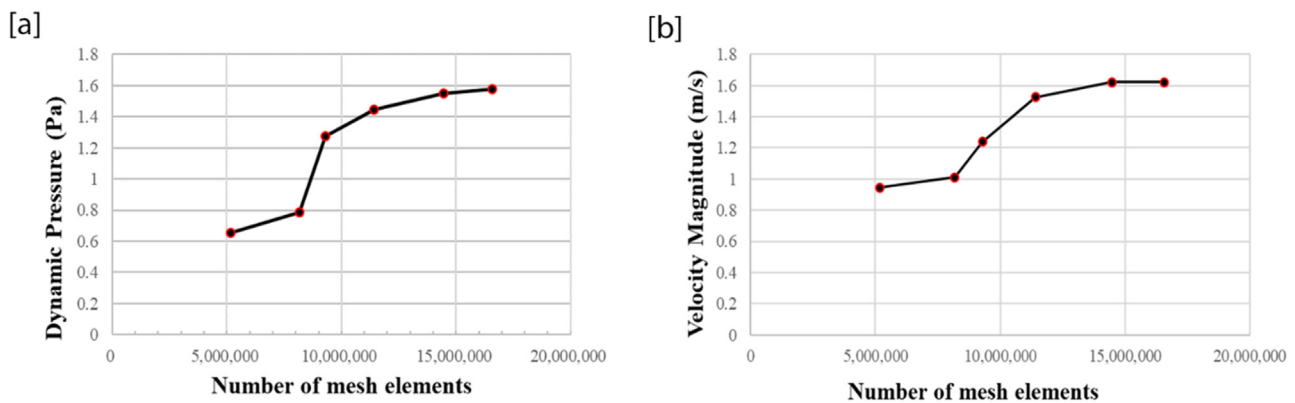


FIG. 5. (a) Dynamic pressure (Pa) at an x - y plane at the bifurcation of gen 0 for six mesh sizes. (b) Velocity magnitude (m/s) at an x - y plane cutting gen 0 for six mesh sizes. Both figures show constant values at around 15×10^6 mesh volume elements.

TABLE II. Air properties used in the simulation for the hot and cool air cases.

Air properties	Hot air	Cool air
Density	1.168 $\frac{\text{kg}}{\text{m}^3}$	1.184 $\frac{\text{kg}}{\text{m}^3}$
Thermal conductivity	0.027 $\frac{\text{W}}{\text{m} \cdot \text{K}}$	0.025 $\frac{\text{W}}{\text{m} \cdot \text{K}}$
Dynamic viscosity	1.932 $\times 10^{-5} \frac{\text{W}}{\text{m} \cdot \text{K}}$	1.849 $\times 10^{-5} \frac{\text{W}}{\text{m} \cdot \text{K}}$
Specific heat	1007 $\frac{\text{J}}{\text{kg} \cdot \text{K}}$	1007.5 $\frac{\text{J}}{\text{kg} \cdot \text{K}}$
Thermal expansion coefficient	0.0032 $\frac{1}{\text{K}}$	0.0034 $\frac{1}{\text{K}}$

$$\frac{\partial \mathbf{u}}{\partial t} + (\mathbf{u} \cdot \nabla) \mathbf{u} = -\frac{1}{\rho} \nabla p + \nu \nabla^2 \mathbf{u} + \frac{\mathbf{F}}{\rho}. \quad (2)$$

Here, \mathbf{u} (m/s) is the local velocity of air, p (Pa) is the pressure, ν (m²/s) is the kinematic viscosity, \mathbf{F} (N) is the sum of any body forces such as gravity, and ρ (kg/m³) is the air density where $\rho = \rho_0 - \alpha \rho_0 (T - T_0)$ with α (1/K) being the air thermal expansion coefficient and $T - T_0$ (K) the temperature difference between air and the lung surface.

Energy equation:

$$\frac{\partial}{\partial t} (\rho E) + \nabla \cdot (\mathbf{u}(\rho E + p)) = \nabla \cdot \left(k_{\text{eff}} \nabla T - \sum_j h \mathbf{J} + (\bar{\tau}_{\text{eff}} \cdot \mathbf{u}) \right), \quad (3)$$

where E (Joule) = $h - \frac{p}{\rho} + \frac{u^2}{2}$ with h being the specific enthalpy calculated using the formula $h = \int_{T_{\text{ref}}}^T c_p dT$. The right-hand side of the equation represents the energy transfer due to conduction, species diffusion, and viscous dissipation. The k_{eff} (W/m·K), T (K), $\bar{\mathbf{J}}$ (kg/m²·s), and $\bar{\tau}_{\text{eff}}$ terms are the effective conductivity, temperature, diffusion flux, and stress tensor, respectively.

V. VALIDATION

For validation, the lung wall pressure contours at 0.4s during inhalation and 3.4s during exhalation are compared with the results measured by Qi et al. (2017), as shown in Fig. 6. The study considers a laminar airflow with a user-defined function for the airflow flow rate, which corresponds to a total breathing cycle of 5.1 s, a tidal volume of 500 ml, and an inspiratory/expiratory ratio of 1:2. During inhalation at 0.4 s [Fig. 6(a)], both models show negative pressure values decreasing gradually from -0.3 to -16.09 Pa as the generation number increases. The negative pressure indicates the suction of air that initiates inhalation in the lungs. The increased negative pressure at distal generations represents the movement of air from higher pressure regions to lower pressure regions. At 3.4s during exhalation, maximum positive pressure is recorded at distal generations creating the necessary driving pressure to remove air from the lungs [Fig. 6(b)]. The model of

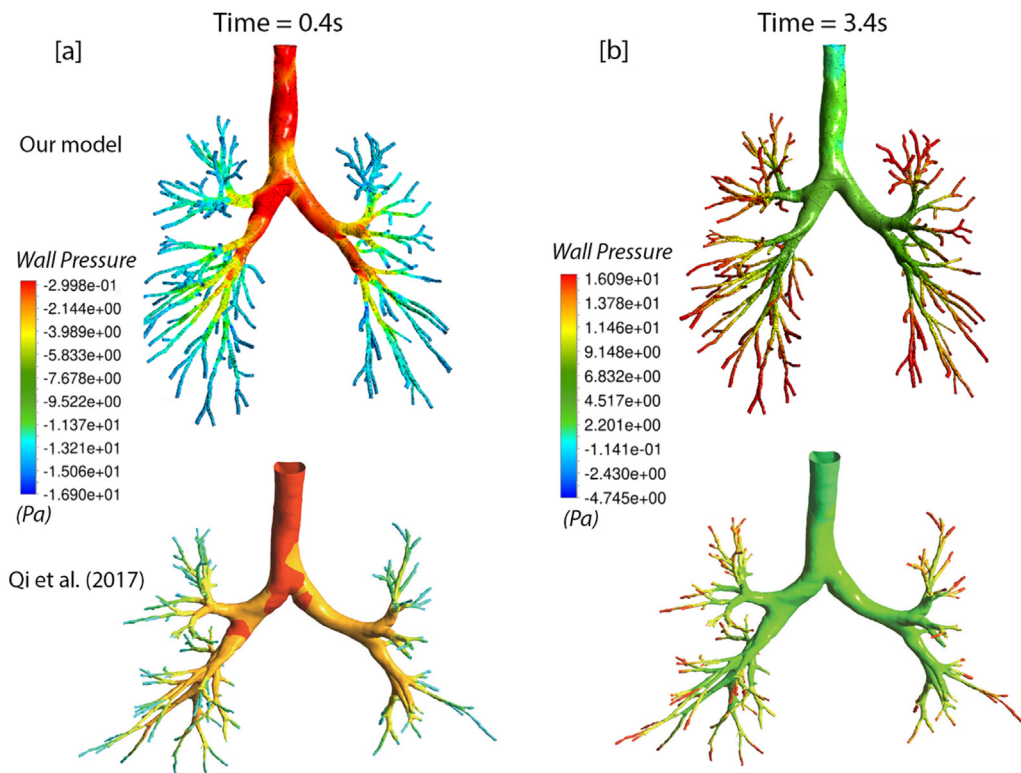


FIG. 6. (a) Comparison in wall pressure (Pa) between our model and Qi et al. (2017) during inhalation at 0.4 s. (b) During exhalation at 3.4 s, for validation of our model where the wall pressure represents the outermost fluid (air) layer near the inner lung surface.

Qi *et al.* (2017) contains a smaller number of generations which explain the extended decreased pressure at distal generations in our model. At 3.4 s, higher compatibility between the contours of the two models is shown. Pressure is almost constant for the first few generations, with values ranging between 3 and 8 Pa, while it exhibits higher values near the periphery at distal generations.

VI. RESULTS AND DISCUSSION

A. Cool air flowing into the lungs

1. Temperature streamlines

Figures 7 and 8 illustrate the temperature streamlines within the human bronchial tree when inhaling cool air. The term temperature streamlines refer to streamlines of air colored according to the temperature degree. Ten instantaneous screenshots at ten different instances “A to J” are chosen from the inhalation cycle of 1.75 s. Figure 7 displays the first five samples where cool air with a temperature of 298 K enters the trachea. The lung surface temperature is set to 310 K, the average human body temperature (37 °C). As the cool air flows in at 0.05 s [A], heat transfer with the lung surface (via convection) occurs where the hot lung surface temperature transfers heat to the cool air. From the trachea [A] to generation 1 [E], the heated air shows an increased temperature reaching a value around 307 K near the lung surface. Figure 8 demonstrates another set of five samples where cold air enters the lung after generation 1. From 0.35 s [F], the cool temperature region expands at a much faster rate, reaching the third generation at 0.45 s [G] and the sixth generation at 0.75 s [H]. Starting from

[H] to 1.7 s [I] and 1.74 s [J], temperature streamlines in all 16 generations gain additional temperature from the lung surface, increasing the volume temperature to around 305 K and the near-surface temperature to more than 307 K. At the time 1.7 s [I], the inhalation velocity, which is in the middle of the deceleration stage, gives rise to vortices in generation 0 (trachea), and streamlines are no longer uniform and smooth. At 1.74 s [J], this phenomenon is more obvious as the inhalation phase ends and the exhalation phase begins, thus reversing the flow direction. Additionally, the air temperature reaches 310 K, mainly in generation 0, due to the effect of the vortices and the increased heat transfer with the lung surface. Due to the presence of vortices, a more turbulent flow occurs, which leads to a higher heat transfer coefficient and heat transfer rate between the two different lung and air temperatures.

2. Volume temperature

Figure 9 shows the variation of the volume temperature inside the lungs throughout the breathing cycle. At time 0 s, cool air is still at the beginning of generation 0, making the lung surface temperature (310 K) the dominant temperature. From 0 to 0.45 s, the temperature drops from 310 to 303 K as the cool air flows [Figs. 7 and 8(a)–8(g)]. Since the volume of generations 0 to 2 constitutes a large percentage of the total volume, the temperature change in these regions significantly influences the volume temperature. The decrease in the volume temperature decelerates after 0.5 s, maintaining a temperature around 302.4 K until 1.5 s (near the end of the inhalation phase). The volume

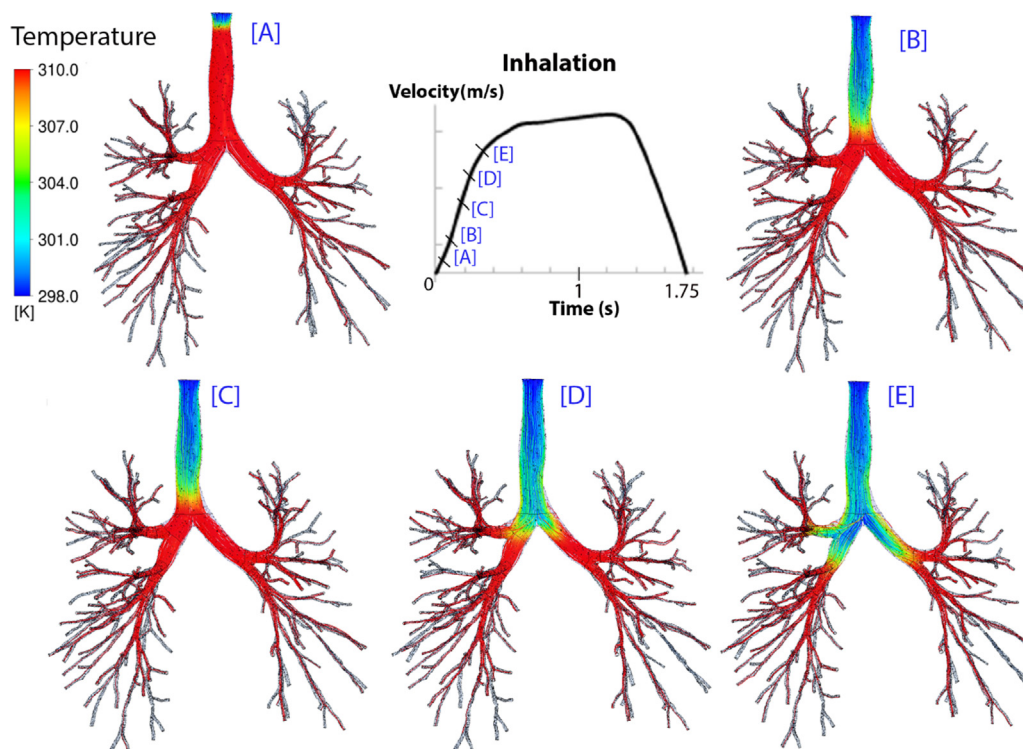


FIG. 7. Temperature streamlines upon inhalation of cool air with a temperature of 298 K, at five different times in the first half of the inhalation phase, where [A] = 0.05 s, [B] = 0.15 s, [C] = 0.2 s, [D] = 0.25 s, and [E] = 0.3 s.

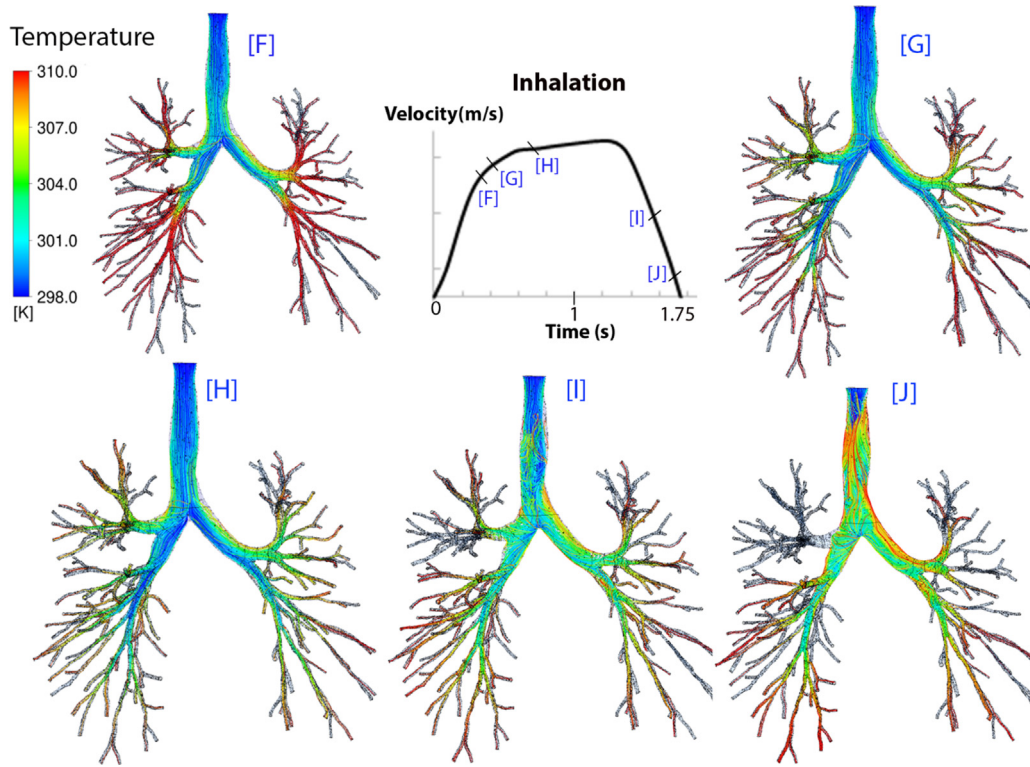


FIG. 8. Temperature streamlines upon inhalation of cool air at five different times during the second half of the inhalation phase, where [F] = 0.35 s, [G] = 0.45 s, [H] = 0.75 s, [I] = 1.7 s, and [J] = 1.74 s.

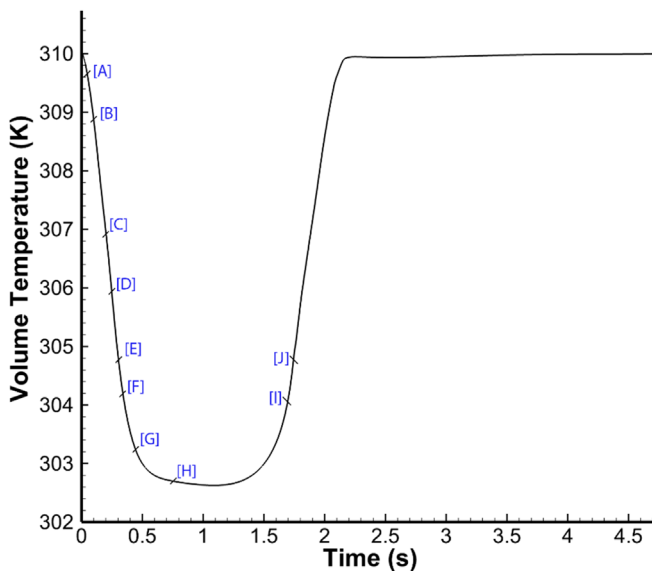


FIG. 9. Air volume temperature change inside the lung during one breathing cycle of 4.75 s in the cool air inhalation case.

temperature experienced little change because the generations after the main bronchi take up a small percentage of the total volume. Therefore, the volume temperature only decreased by less than 0.5 K as the cool air reached deeper generations. After 1.5 s, the volume temperature rises back to 310 K within half a second, where the initial increase in the temperature was explained previously in Figs. 8(i) and 8(j). The gradual increase in temperature after 1.7 s is due to the exhalation of cool air out of the lungs. At 2.2 s, the less cooled air (higher than its initial inlet temperature) is completely exhaled. As a result, the volume temperature (which now represents the lung temperature solely) returns gradually to 310 K until the next inhalation phase begins.

3. Surface heat flux and surface temperature

Surface heat flux (W/m^2) and surface temperature (K) variations for the surfaces of generations 0–15 upon the inhalation and exhalation of cool air are shown in Figs. 10(a) and 10(b), respectively. In Fig. 10(a), the breathing velocity profile is shown with positive velocity values during inhalation from 0 to 1.75 s and negative values referring to the reversing of flow direction during exhalation from 1.75 to 4.75 s. The surface heat flux for all generations considers the convective heat transfer, which is computed by FLUENT at each time step using the formula $q'' = h(T - T_{ref})$, with h being the enthalpy, T the varying

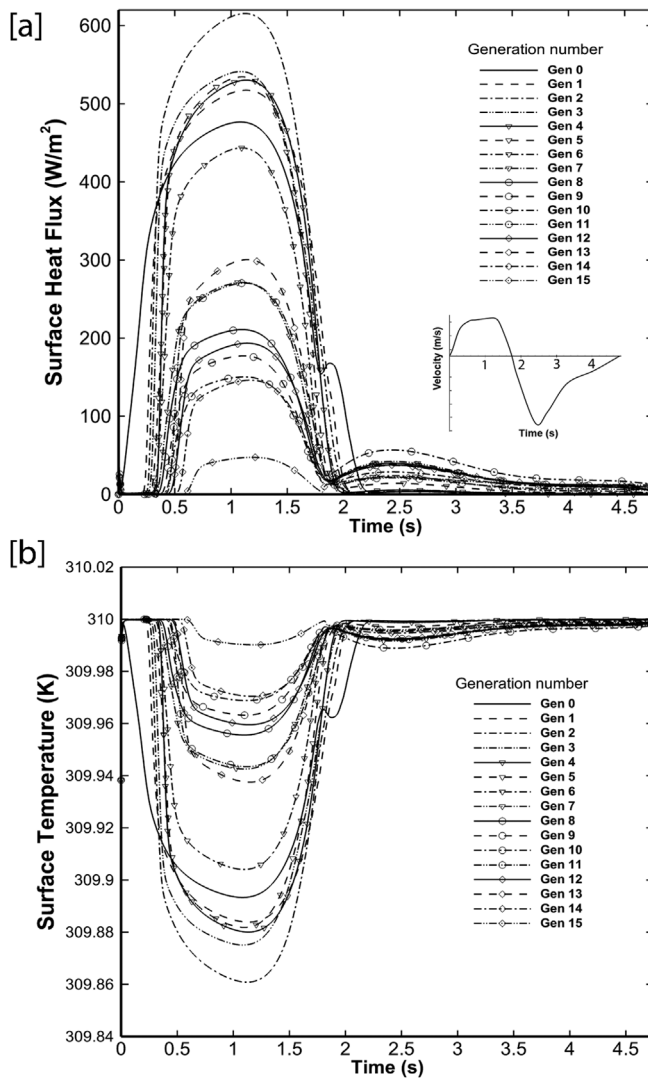


FIG. 10. (a) Surface heat flux (W/m^2) with the velocity breathing profile and (b) surface temperature (K) variation for all generations during inhalation and exhalation upon inhaling cool air. The term “surface” refers to the outermost air layer near the inner lung surface.

air temperature, and T_{ref} the reference temperature taken to be 310 K (lung temperature). The term surface temperature is the outermost fluid layer adjacent to the lung surface that is modeled by shell conduction. The surface heat flux shows a rapid increase toward the middle of the inhalation phase, followed by a rapid decrease toward the end of inhalation. At the beginning of exhalation, a slight rise in the surface heat flux values is followed by a gradual decline toward the end of exhalation. This pattern follows the inhalation velocity profile where the surface heat flux increases with air velocity and decreases to 0 at the end of inhalation (due to static air). During exhalation, shallow values appear as air leaves the lung and heat transfer ceases. Gen 2 shows the highest surface heat flux value during inhalation reaching $620 W/m^2$, a 93.55% increase from gen 5 ($40 W/m^2$).

Interestingly, the surface heat flux of all generations roughly saturates into two clusters during inhalation, with a minimum gap of $150 W/m^2$ [Fig. 10(a)]. During inhalation, the upper cluster with maximum surface heat fluxes ranging from 450 to $620 W/m^2$ consists of generations 0, 1, 2, 3, 4, 5, and 6. The lower cluster with maximum surface heat fluxes ranging from 50 to $300 W/m^2$ consists of generations 7, 8, 9, 10, 11, 12, 13, 14, and 15. This grouping is due to the high-temperature difference ΔT between the hot lung surface and the cool air (directly proportional to the surface heat flux) in the generations of the upper cluster and the low-temperature difference for the generations of the lower cluster. This is shown in Fig. 10(b), where proximal generations (gen 0–6) exhibit low surface temperature values and distal generations (gen 7–15) display higher surface temperatures. As cool air enters the lung from the inlet of gen 0, heat transfer begins, and the air temperature gradually increases as it passes from one generation to the other. The increased air temperature leads to a reduced temperature difference and, thus, reduced surface heat flux values in the distal generations. In each cluster, the hierarchy of the generations and the large heat flux values depend on another parameter, the heat transfer coefficient h ($W/m^2 \cdot K$), which is directly proportional to the surface heat flux. This parameter varies proportionally with the turbulence of the flow and the generation of vortices. As a result, as the flow progresses from the trachea to distal generations, the turbulence effect decreases due to friction (shell conduction forming a solid layer that represents the lung surface). Thus, the heat transfer coefficient and heat flux decrease with increased generation number.

Figure 11 shows vorticity contours at a cross-section T1 at the center of the trachea (gen 0), where high vorticity values, leading to high heat transfer coefficients and high surface heat fluxes [also shown in Fig. 10(a)], are expected due to the turbulence of the flow. While the laryngeal jet moves downstream through the trachea, the force imbalance of the fast-moving glottides jet from the anterior wall and relatively slow-moving air from the posterior wall creates a pair of counter-rotating vortices across a transverse plane of the trachea (T1 in Fig. 11). The development of such vortices is shown at different time instants in Fig. 11. Initially, two counter-rotating vortices start forming at $t = 0.65$ s near the dorsal region of the tracheal wall (T1) and slowly build up until maximum vorticity is reached around $1385 s^{-1}$. At the end of inhalation at 1.7 s, as the velocity of air reaches 0 m/s, the intensity of the vortex cores reduces, and vorticity values decrease immensely before starting to increase again during the exhalation phase (2–3 s). This latter phenomenon is also shown in Figs. 10(a) and 10(b), where the increasing vorticity values in the exhalation phase at 2 s slightly increase the surface heat coefficients and the surface heat fluxes. Moreover, gen 0 exhibits different behavior than other generations [Figs. 10(a) and 10(b)] at the onset of heat transfer due to its increased length compared to further generations. The surface temperature variation and, therefore, surface heat flux variation start from 0 s for gen 0, unlike further generations that start at around 0.2 s [also shown in Fig. 7(d)].

B. Hot air flowing into lungs

1. Temperature streamlines

Temperature streamlines within the human bronchial tree when inhaling hot air are shown in Figs. 12 and 13 for the first half of the inhalation phase and the second half of the inhalation phase,

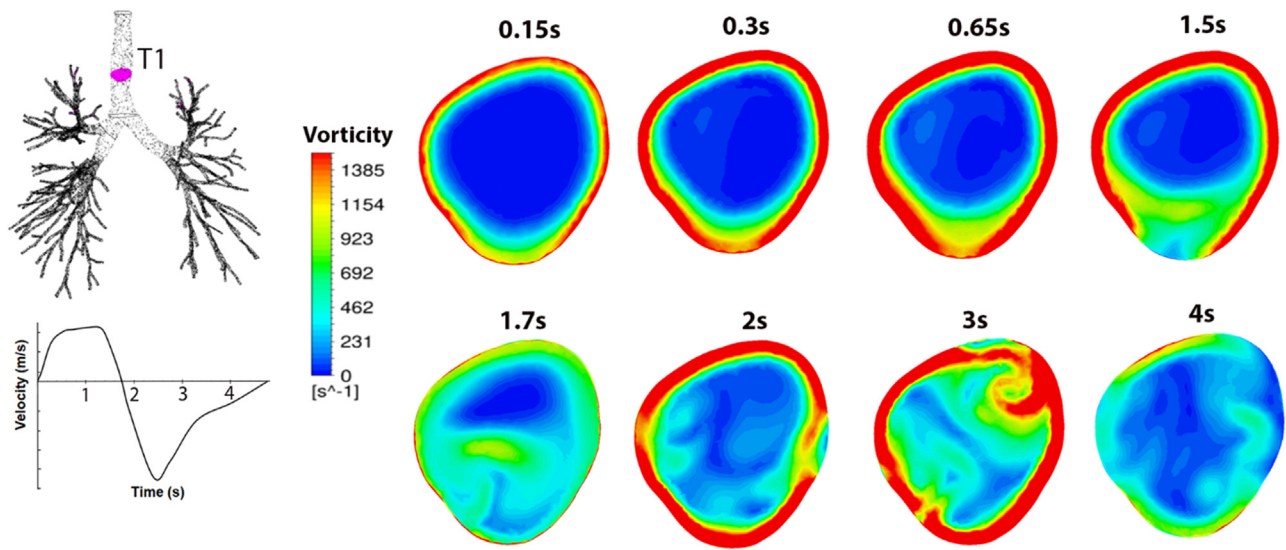


FIG. 11. The development of the vorticity field throughout the breathing cycle at a cross-section T1 at the middle of gen 0 of the lung.

respectively. Ten instantaneous snapshots at ten different times “A to J” are selected from the inhalation phase. Hot air with a temperature of 316 K enters the trachea of the lung. As the cool air case, heat transfer occurs between the lung surface ($37^{\circ}C$) and the hot air. However,

unlike the cool air case, the hot air loses heat to the lung surface, and thus, its temperature decreases gradually. Figure 12 displays the penetration of the hot air from generation 0 at 0.05 s [A] to generation 2 at 0.3 s [E]. The hot air temperature decreases from 316 K to around

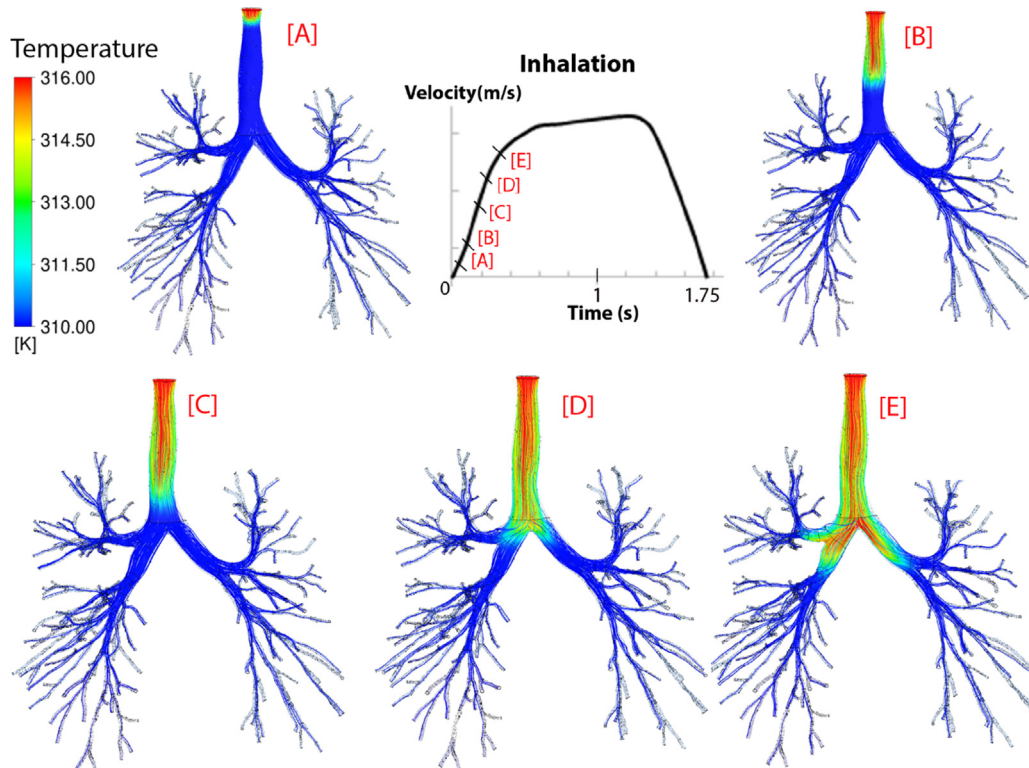


FIG. 12. Temperature streamlines upon inhalation of hot air with a temperature of 316 K, at five different times during the first half of the inhalation phase, where [A] = 0.05 s; [B] = 0.15 s; [C] = 0.2 s; [D] = 0.25 s; and [E] = 0.3 s.

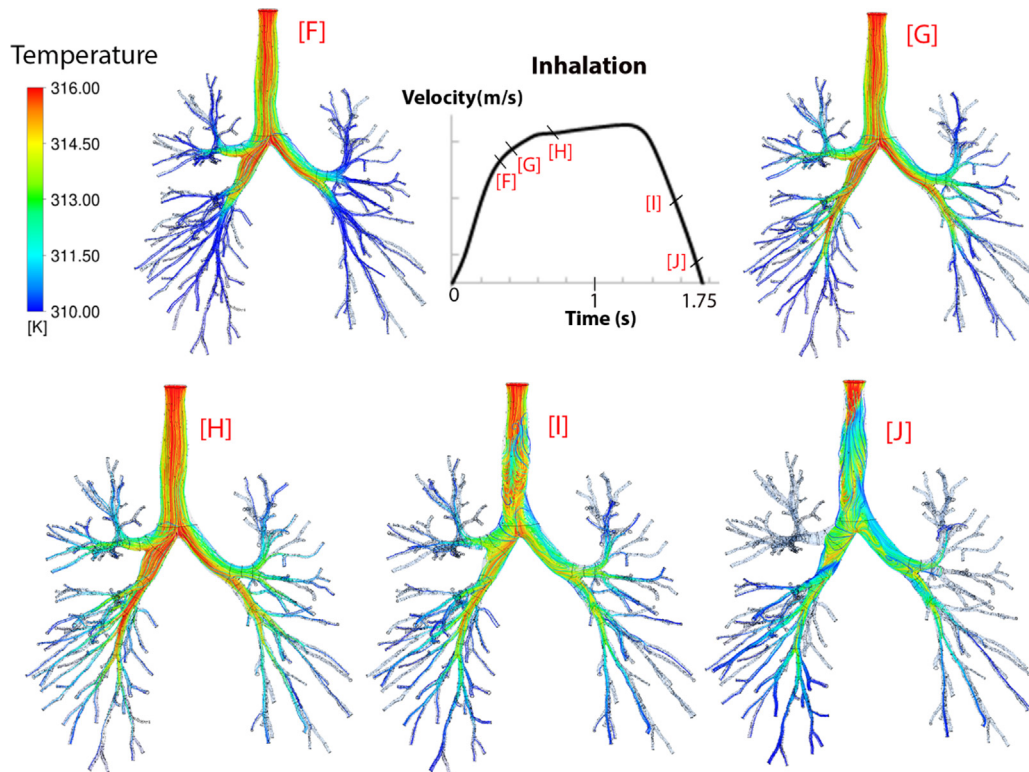


FIG. 13. Temperature streamlines upon inhalation of hot air at five different times during the second half of the inhalation phase, where [F] = 0.35 s; [G] = 0.45 s; [H] = 0.75 s; [I] = 1.7 s; and [J] = 1.74 s.

311.5 K near the lung surface. Figure 13 shows the penetration of the temperature streamlines into deeper generations, starting from 0.35 s [F] to 1.74 s [J] at the end of inhalation, where the temperature reaches its coolest value at around 310 K.

2. Volume temperature

Figure 14 demonstrates the lung volume temperature variation during inhalation and exhalation. Like the cool air case, at time 0 s, the lung surface temperature (310 K) is the prevalent temperature. As the hot air starts to occupy the lung volume, heat transfer with the lung surface increases the volume temperature from 310 K to slightly above 313.5 K ([A] to [H]). From 0.5 s to 1.5 s, the rate of heat transfer decreases, and the volume temperature maintains a constant value of around 313.6 K. After 1.5 s, exhalation of air out of the lung begins, and the volume temperature gradually falls back to the lung surface temperature (310 K).

3. Surface heat flux and surface temperature

In the cool air case, the surface heat flux (W/m²) and surface temperature (K) fluctuations for the surfaces of all generations upon the inhalation and exhalation of hot air are shown in Figs. 15(a) and 15(b),

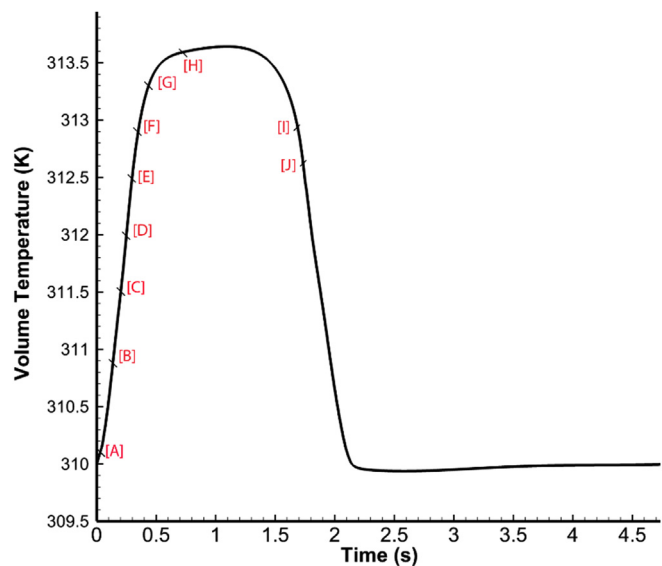


FIG. 14. Air volume temperature change inside the lung during one breathing cycle of 4.75 s in the hot air inhalation case.

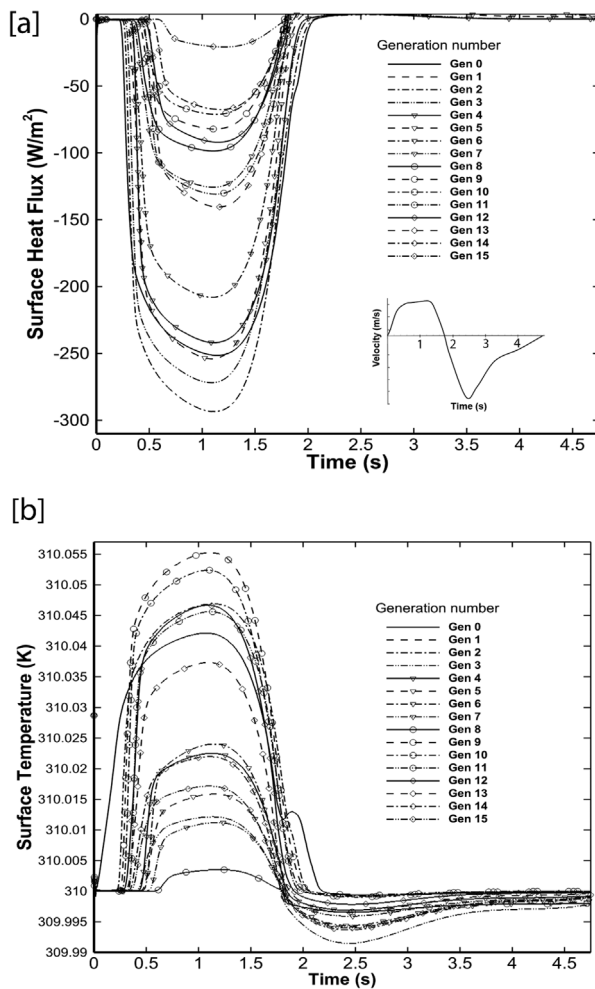


FIG. 15. (a) Surface heat flux (W/m^2) with the velocity breathing profile and (b) surface temperature (K) variation for all generations during inhalation and exhalation in the hot air inhalation case. The term “surface” refers to the outermost air layer near the inner lung surface.

respectively. For all generations, the surface heat flux shows a steep decrease from 0 s reaching around -250 W/m^2 at 0.4 s. The negative values indicate that heat transfer occurs from the fluid to the wall boundary (lung surfaces). Maximum absolute values of around 290 W/m^2 are reached at 1 s when the air velocity comes to its highest during the inhalation phase. After 1.2 s, absolute surface heat flux values show a rapid decrease to 0 W/m^2 at the beginning of exhalation. The two clusters of generations and their hierarchy are the same as in the cool air case, with gen 2 displaying the highest absolute surface heat flux and gen 15 showing the lowest (maximum around 20 W/m^2). However, the grouping and hierarchy for the surface temperature are not similar to the cool air case [Fig. 15(b)]. The variation in the surface temperature from its initial temperature (310 K) is minimal for all generations, with values ranging from 310.002 to 310.058 K. Generations 9 and 10 display the maximum increased temperature at around 310.055 K, while generation 8 shows the lowest increased temperature at around 310.002 K.

VII. CONCLUSION

First, temperature streamlines for both cases demonstrated similar patterns during inhalation. Since the hot air is 6°C higher than the lung surface temperature and the cold air is 12°C lower, it can be concluded that the airflow temperature patterns depend on the inlet breathing velocity profile instead of the temperature difference between air and the lung surface. Second, doubling this temperature difference in the cool air case compared to the hot one was directly correlated with the volume temperature change. The maximum volume temperature variation occurred with a temperature difference of 7 K for the cool air case vs a maximum of 3.5 K for the hot air case. Third, the absolute surface heat flux values showed a maximum increase of 620 W/m^2 for the cool air case vs 290 W/m^2 for the hot air case. As the maximum variation in the surface heat flux decreased by over 50% from the hot air case to the cold one, it can be concluded that the surface heat flux is dependent not only on the temperature difference but also on the heat transfer coefficient. The density, viscosity, thermal conductivity, and specific heat of hot air affect the Reynolds number, the Nusselt number, the heat transfer coefficient, and the surface heat flux.

Heat transfer between inhaled hot or cool air and the lung surface occurs in the first few generations. In reality, on the surface of the lung resides a surfactant layer which is naturally produced by alveolar cells to lower the air–liquid surface tension. Due to the heat transfer between the moving fluid (air) and the static fluid (surfactant), the lung can be considered an *in vivo* heat exchanger, balancing the inhaled air temperature by lowering the hot air temperature and increasing the cool air temperature. The lack of this balanced temperature as air moves farther into the alveolar regions may induce alveolar thermal stresses, especially in extreme air temperatures. Therefore, air movement across all generations for a long distance before reaching the alveoli is crucial for regulating the temperature and avoiding alveolar injuries.

ACKNOWLEDGMENTS

The authors would like to acknowledge the computing facility at the University of Technology Sydney (UTS). This research did not receive any specific grant from funding agencies in the public, commercial, or not-for-profit sectors.

AUTHOR DECLARATIONS

Conflict of Interest

The authors have no conflicts to disclose.

Author Contributions

Suvash C. Saha: Conceptualization (equal); data curation (equal); methodology (equal); project administration (equal); software (equal); supervision (equal); writing – review & editing (equal). **Isabella Francis:** Investigation (equal); methodology (equal); resources (equal); software (equal); validation (equal); visualization (equal); Writing – original draft (equal). **Xinlei Huang:** Data curation (equal); methodology (supporting); software (supporting); validation (supporting); writing – review & editing (supporting). **Akshoy Ranjan Paul:** Formal analysis (supporting); writing – review & editing (supporting).

DATA AVAILABILITY

The data that support the findings of this study are available within the article.

REFERENCES

- Chekan, E. G., Cummings, J. F., Mabe, I., Hunter, S., and Clymer, J. W., "Thickness of cadaveric human lung tissue," *Surg. Technol. Int.* **29**, 207–213 (2016).
- Chen, X., Ma, R., Zhong, W., Sun, B., and Zhou, X., "Numerical study of the effects of temperature and humidity on the transport and deposition of hygroscopic aerosols in a G3–G6 airway," *Int. J. Heat Mass Transfer* **138**, 545–552 (2019).
- Daviskas, E., Gonda, I., and Anderson, S. D., "Mathematical modeling of heat and water transport in human respiratory tract," *J. Appl. Physiol.* **69**(1), 362–372 (1990).
- Faizal, W., Ghazali, N. N. N., Khor, C., Badruddin, I. A., Zainon, M., and Yazid, A. A., *et al.* "Computational fluid dynamics modelling of human upper airway: A review," *Comput. Methods Programs Biomed.* **196**, 105627 (2020).
- Ferron, G. A., Haider, B., and Kreyling, W. G., "Inhalation of salt aerosol particles—I. Estimation of the temperature and relative humidity of the air in the human upper airways," *J. Aerosol Sci.* **19**(3), 343–363 (1988).
- Finlay, W. H., and Stapleton, K. W., "The effect on regional lung deposition of coupled heat and mass transfer between hygroscopic droplets and their surrounding phase," *J. Aerosol Sci.* **26**(4), 655–670 (1995).
- Hanna, L. M., and Scherer, P. W., "A theoretical model of localized heat and water vapor transport in the human respiratory tract," *J. Biomech. Eng.* **108**(1), 19–27 (1986).
- Iasiello, M., Andreozzi, A., Bianco, N., and Vafai, K., "The porous media theory applied to radiofrequency catheter ablation," *Int. J. Numer. Methods Heat Fluid Flow* **30**, 2669 (2020).
- Iasiello, M., Vafai, K., Andreozzi, A., and Bianco, N., "Hypo-and hyperthermia effects on LDL deposition in a curved artery," *Comput. Therm. Sci.* **11**(1–2), 95 (2019).
- Ingenito, E. P., Solway, J., McFadden, E. R., Jr., Pichurko, B. M., Cravalho, E. G., and Drazen, J. M., "Finite difference analysis of respiratory heat transfer," *J. Appl. Physiol.* **61**(6), 2252–2259 (1986).
- Islam, M. S., Larpruenrudee, P., Paul, A. R., Paul, G., Gemci, T., Gu, Y., and Saha, S. C., "SARS CoV-2 aerosol: How far it can travel to the lower airways?," *Phys. Fluids* **33**(6), 061903 (2021a).
- Islam, M. S., Larpruenrudee, P., Saha, S. C., Pourmehrhan, O., Paul, A. R., Gemci, T., *et al.* "How severe acute respiratory syndrome coronavirus-2 aerosol propagates through the age-specific upper airways," *Phys. Fluids* **33**(8), 081911 (2021b).
- Keangin, P., and Rattanadecho, P., "Analysis of heat transport on local thermal non-equilibrium in porous liver during microwave ablation," *Int. J. Heat Mass Transfer* **67**, 46–60 (2013).
- Keangin, P., Vafai, K., and Rattanadecho, P., "Electromagnetic field effects on biological materials," *Int. J. Heat Mass Transfer* **65**, 389–399 (2013).
- Keck, T., Leiacker, R., Riechelmann, H., and Rettinger, G., "Temperature profile in the nasal cavity," *Laryngoscope* **110**(4), 651–654 (2000).
- Kulkarni, N. A., and Kleinstreuer, C., "High-temperature effects on the mucus layers in a realistic human upper airway model," *Int. J. Heat Mass Transfer* **163**, 120467 (2020).
- Kumar, B., Srivastav, V. K., Jain, A., and Paul, A. R., "Study of numerical schemes for the CFD simulation of human airways," *Int. J. Integr. Eng.* **11**(8), 32–40 (2019).
- Larpruenrudee, P., Islam, M. S., Paul, G., Paul, A. R., Gu, Y., and Saha, S. C., "Model for Pharmaceutical aerosol transport through stenosis airway," *Handbook of Lung Targeted Drug Delivery Systems: Recent Trends and Clinical Evidences* (2022), pp. 91–128.
- Pan, S.-Y., Ding, M., Huang, J., Cai, Y., and Huang, Y.-Z., "Airway resistance variation correlates with prognosis of critically ill COVID-19 patients: A computational fluid dynamics study," *Comput. Methods Programs Biomed.* **208**, 106257 (2021).
- Paul, A. R., Khan, F., Jain, A., and Saha, S. C., "Deposition of smoke particles in human airways with realistic waveform," *Atmosphere* **12**(7), 912 (2021).
- Primiano, F. P., Jr., Sidel, G. M., Montague, F. W., Jr., Kruse, K. L., Green, C. G., and Horowitz, J. G., "Water vapour and temperature dynamics in the upper airways of normal and CF subjects," *Eur. Respir. J.* **1**(5), 407–414 (1988).
- Qi, S., Zhang, B., Teng, Y., Li, J., Yue, Y., Kang, Y., and Qian, W., "Transient dynamics simulation of airflow in a CT-scanned human airway tree: More or fewer terminal bronchi?," *Comput. Math. Methods Med.* **2017**, 1969023.
- Shukla, S. K., Srivastav, V. K., Paul, A. R., and Jain, A., "Computational study of aerosol drug deposition on tumorous human airway model," in *Proceedings of the Fortieth national Conference on Fluid Mechanics and Fluid Power* (2013).
- Singh, D., Jain, A., and Paul, A. R., "Numerical study on particle deposition in healthy human airways and airways with glomus tumor," in *Advances in Biomedical Engineering and Technology* (Springer, 2021) p. 379–90.
- Srivastav, V. K., Jain, A., Paul, A. R., and Joshi, S., "CFD modelling of airflow in human respiratory system," in *International Conference on Mechanical Engineering* (2011).
- Srivastav, V. K., Paul, A. R., and Jain, A., "Computational fluid dynamics study of airflow and particle transport in third to sixth generation human respiratory tract," *International Journal of Emerging Multidisciplinary Fluid Sciences* **3**(4), 227–234 (2011).
- Srivastav, V. K., Kumar, B., Jain, A., and Paul, A. R. A., "Computational study on airflow in human respiratory tract at normal and heavy breathing conditions," in *Proceedings of the 6th International and 43rd National Conference on Fluid Mechanics and Fluid Power* (FMFP, 2016).
- Srivastav, V. K., Paul, A. R., and Jain, A., "Capturing the wall turbulence in CFD simulation of human respiratory tract," *Mathematics and computers in simulation* **160**, 23–38 (2019).
- Srivastav, V. K., Paul, A. R., and Jain, A., "Computational study of drug delivery in tumorous human airways," *International Journal of Computing Science and Mathematics* **10**(5), 459–75 (2019).
- Srivastav, V. K., Shukla, R. K., Paul, A. R., and Jain, A., "Computational study on the effect of human respiratory wall elasticity," *Int. J. Biomed. Eng. Technol.* **37**(1), 46–64 (2021).
- Tawhai, M. H., and Hunter, P. J., "Modeling water vapor and heat transfer in the normal and the intubated airways," *Ann. Biomed. Eng.* **32**(4), 609–622 (2004).
- Tsu, M. E., Babb, A. L., Ralph, D. D., and Hlastala, M. P., "Dynamics of heat, water, and soluble gas exchange in the human airways: 1. A model study," *Ann. Biomed. Eng.* **16**(6), 547–571 (1988).
- Tiwari, A., Paul, A. R., Jain, A., and Saha, S. C., "Evaluation of the design of efficient dry powder inhalers," in *Handbook of Lung Targeted Drug Delivery Systems: Recent Trends and Clinical Evidences*, edited by Pathak, Y. and Islam, N. (CRC Press, Boca Raton, Florida, 2022). Chap. 9.
- Tiwari, A., Jain, A., Paul, A. R., and Saha, S. C., "Computational evaluation of drug delivery in human respiratory tract under realistic inhalation," *Phys. Fluids* **33**(8), 083311 (2021).
- Tiwari, A., Sharma, S., Srivastav, V. K., Jain, A., and Paul, A. R., "Computational study of atomization models and optimal design of a pressurized inhaler," *J. Biomim. Biomater. Biomed. Eng.* **50**, 123–134 (2021).
- Van Dyk, J., Keane, T., and Rider, W., "Lung density as measured by computerized tomography: Implications for radiotherapy," *Int. J. Radiat. Oncol. Biol. Phys.* **8**(8), 1363–1372 (1982).
- Wu, D., Tawhai, M. H., Hoffman, E. A., and Lin, C. L., "A numerical study of heat and water vapor transfer in MDCT-based human airway models," *Ann. Biomed. Eng.* **42**(10), 2117–2131 (2014).
- Xi, J., Kim, J., and Si, X. A., "Effects of nostril orientation on airflow dynamics, heat exchange, and particle depositions in human noses," *Eur. J. Mech.—B/Fluids* **55**, 215–228 (2016).
- Xu, C., Zheng, X., and Shen, S., "A numerical study of the effects of ambient temperature and humidity on the particle growth and deposition in the human airway," *Environ. Res.* **200**, 111751 (2021).
- Yang, D., and Cao, M., "Effect of changes in lung physical properties on microwave ablation zone during respiration," *Biomed. Eng. Lett.* **10**(2), 285–298 (2020).
- Zhang, Z., and Kleinstreuer, C., "Species heat and mass transfer in a human upper airway model," *Int. J. Heat Mass Transfer* **46**(25), 4755–4768 (2003).